Mathematics and Computers in Simulation 233 (2025) 296–310

Contents lists available at ScienceDirect

Mathematics and Computers in Simulation

journal homepage: www.elsevier.com/locate/matcom

Original articles

On L^2 approximation by planar Pythagorean-hodograph curves

Rida T. Farouki [a], Marjeta Knez [b,c], Vito Vitrih [d,e,*], Emil Žagar [b,c]

[a] Mechanical & Aerospace Engineering, University of California, Davis, CA 95616, USA
[b] Faculty of Mathematics and Physics, University of Ljubljana, Jadranska 19, Ljubljana, Slovenia
[c] Institute of Mathematics, Physics and Mechanics, Jadranska 19, Ljubljana, Slovenia
[d] Faculty of Mathematics, Natural Sciences and Information Technologies, University of Primorska, Glagoljaška 8, Koper, Slovenia
[e] Andrej Marušič Institute, University of Primorska, Muzejski trg 2, Koper, Slovenia

ARTICLE INFO

MSC:
65D05
65D07
65D17

Keywords:
L^2 approximation
Complex polynomial
Pythagorean-hodograph curve
Pythagorean-hodograph spline
Preimage

ABSTRACT

The L^2 approximation of planar curves by Pythagorean-hodograph (PH) polynomial curves is addressed, based on the distance defined by a metric for planar curves represented as complex-valued functions of a real parameter. Because of the nonlinear nature of polynomial PH curves, constructing L^2 approximants involves solving a nonlinear optimization problem. However, a simplified method that requires only the solution of a linear system may be developed by formulating the L^2 approximation in the preimage space. The extension of the methodology to approximation by PH B-spline curves is also addressed, and several examples are provided to illustrate its implementation and potential.

1. Introduction

A polynomial Pythagorean-hodograph (PH) curve $\mathbf{r}(t)$ is distinguished by the property that its *parametric speed* $\sigma(t) = |\mathbf{r}'(t)|$ — the derivative $\mathrm{d}s/\mathrm{d}t$ of the curve arc length s with respect to the parameter t — is a *polynomial*. This distinctive feature permits exact computation of various curve properties that necessitate numerical approximations for "ordinary" polynomial curves [1]. Further background on the PH curves may be found in [2,3].

The construction and analysis of PH curves may be greatly facilitated by adopting suitable algebraic models for their representation. For planar PH curves the complex variable model [4], in which points (x, y) in the Euclidean plane are identified with the complex numbers $x+\mathrm{i}\,y$, serves this purpose. For spatial PH curves, models based upon the quaternion algebra or the Hopf map from $\mathbb{R}^4$ to $\mathbb{R}^3$ ensure a representation that is invariant with respect to the chosen orientation of the Euclidean coordinate axes, [5,6].

The nonlinear nature of PH curves precludes direct specification through the customary "control point" paradigm of computer aided geometric design. Consequently, the typical approach to construct PH curves is through the interpolation of prescribed geometric data — points, tangents, curvatures, etc. — at discrete locations. Examples of these constructions are described in [7–15] for individual planar or spatial PH curve segments, and in [16–19] for planar or spatial PH spline curves. These constructions have been extended to incorporate global constraints — for example, the imposition of prescribed arc lengths on PH curves [20–24] or minimization of the sum of squared distances of PH curve control points from those of a given "target" curve [25,26].

Identifying a planar parametric curve, given by a continuous parameterization, with the graph of a continuous complex-valued function of a real parameter, allows us to define a metric function for planar curves. Specifically, the metric proposed in [27],

* Corresponding author at: Faculty of Mathematics, Natural Sciences and Information Technologies, University of Primorska, Glagoljaška 8, Koper, Slovenia.
E-mail addresses: farouki@ucdavis.edu (R.T. Farouki), marjetka.knez@fmf.uni-lj.si (M. Knez), vito.vitrih@upr.si (V. Vitrih), emil.zagar@fmf.uni-lj.si (E. Žagar).

https://doi.org/10.1016/j.matcom.2025.02.001
Received 8 July 2024; Received in revised form 17 December 2024; Accepted 1 February 2025
Available online 10 February 2025

induced by a certain inner product, offers a way to measure the distance between two planar parametric curves. In [27] this metric was applied to bounded modifications of PH curves, and it was shown that small modifications of the preimage curve imply small changes of the PH curve. This observation motivated the derivation of an algorithm, presented herein, that provides a simple and efficient way to approximate a given C^1 parametric curve with a so-called *alternative* L^2 PH approximant. Namely, if the vector space is equipped with a norm induced by an inner product, a classical way to approximate functions in the vector space by functions in a chosen subspace is to use the L^2 approach. However, applying this kind of approximation to planar Pythagorean-hodograph curves is an approach that has not yet been addressed. Since we lose the linear space structure, the problem becomes highly nonlinear and requires the use of nonlinear optimization solvers to compute the solution. Moreover, there may be difficulties in identifying the global minimum. To circumvent these problems, we propose a method to linearize the problem while keeping the same approximation order as in the nonlinear case. Furthermore, to approximate curves of complicated shape with the alternative L^2 approximants, the construction is generalized to the planar PH B-spline curves, introduced in [25].

Although the focus of the present study is on the approximation of general planar curves by polynomial PH curves, the approach may also apply to various generalizations, such as the rational PH curves [28,29]; PH curves constructed in terms of mixed polynomial/trigonometric bases [30,31]; and PH curves defined with respect to the Minkowski metric [32–34].

The plan for the remainder of this paper is as follows. Section 2 introduces the general problem of L^2 approximation of planar curves, and Section 3 is specialized to the case of approximation by PH curves. The latter context involves solving of a nonlinear optimization problem that necessitates a numerical solution. An alternative approach is proposed in Section 4 based on minimizing the distance between the preimage polynomial of a PH curve and the complex square root of the derivative of the curve to be approximated. This has the advantage of incurring only the solution of a linear system of equations to identify the best approximant. Section 5 extends the methodology to approximation by planar PH B-spline curves. Finally, Section 6 summarizes the key contributions of this study and suggests further extensions and applications of the proposed schemes.

2. L^2 approximation of planar parametric curves

By representing planar parametric curves as loci in the complex plane, it is possible to measure the distance between two planar curves using a *norm* derived from the complex-valued inner product [27]. This further allows us to formulate the L^2 approximation problem for planar parametric curves in a standard way, as in the classical function theory.

We identify points (x, y) in a real plane with complex numbers $x + \mathrm{i}\, y$ and define parametric curves as sets of points given by a parameterization of the form $\mathbf{u} : [0,1] \to \mathbb{C},\ t \mapsto \mathbf{u}(t)$. A planar parametric curve is thus considered as a graph of a complex-valued function. Let $V := C([0,1], \mathbb{C})$ be the vector space of continuous complex-valued functions defined on the interval $[0,1]$. We equip V with the standard inner product

$$\langle \mathbf{u},\, \mathbf{v} \rangle = \int_0^1 \mathbf{u}(t)\overline{\mathbf{v}}(t)\, dt, \tag{1}$$

and define the *norm* on V as $\|\mathbf{u}\| = \sqrt{\langle \mathbf{u},\, \mathbf{u} \rangle}$. Moreover, the distance between two elements $\mathbf{u}, \mathbf{v} \in V$ is defined by

$$\text{distance}(\mathbf{u}, \mathbf{v}) := \|\mathbf{u} - \mathbf{v}\| = \sqrt{\int_0^1 |\mathbf{u}(t) - \mathbf{v}(t)|^2\, dt}. \tag{2}$$

Let $S \subset V$ be a $(n+1)$-dimensional subspace of V. The standard L^2 problem is defined as follows: for a given function $\mathbf{f} \in V$ find $\mathbf{s}^* \in S$ such that

$$\mathbf{s}^* = \underset{\mathbf{s} \in S}{\operatorname{argmin}} \|\mathbf{f} - \mathbf{s}\| .$$

The sufficient and necessary condition for $\mathbf{s}^*$ to be the solution of this optimization problem is that $\mathbf{f} - \mathbf{s}^*$ is orthogonal to S [35]. To construct $\mathbf{s}^*$ we need to choose a basis $\{\varphi_0, \varphi_1, \ldots, \varphi_n\}$ for S. Then $\mathbf{s}^* = \sum_{j=0}^n \mathbf{a}_j \varphi_j$, where the coefficients $\mathbf{a} = (\mathbf{a}_j)_{j=0}^n \in \mathbb{C}^{n+1}$ are the solution of a Gram system $G\,\mathbf{a} = \mathbf{g}$, with $G = \left(\langle \varphi_k,\, \varphi_j \rangle\right)_{j,k=0}^n$ and $\mathbf{g} = \left(\langle \mathbf{f},\, \varphi_j \rangle\right)_{j=0}^n$. If $\{\varphi_j\}_{j=0}^n$ is an orthonormal basis, the solution is given in the simple closed form as $\mathbf{s}^* = \sum_{j=0}^n \langle \mathbf{f},\, \varphi_j \rangle\, \varphi_j$.

Consider first S as a space of polynomials of fixed degree n. We denote by $\mathbb{P}_n = \mathbb{P}_n(\mathbb{R})$ and $\mathbb{P}_n(\mathbb{C})$ real-valued and complex-valued polynomials of degree n in a real variable, respectively. Later, we will also consider polynomial splines. An appropriate basis for representing parametric polynomial curves of degree n is the Bernstein basis, defined by

$$b_k^n(t) = \binom{n}{k} t^k (1-t)^k, \quad k = 0, 1, \ldots, n.$$

An orthonormal basis concerning the inner product (1) is given by the Legendre polynomials L_k, $k = 0, 1, \ldots, n$, which may be expressed in terms of the Bernstein basis [36] as

$$L_k(t) = \sqrt{2k+1} \sum_{i=0}^k (-1)^{k+i} \binom{k}{i} b_i^k(t). \tag{3}$$

The following example illustrates the construction of the polynomial curve that approximates a given planar curve in the L^2 sense described above.

Table 1
The distances of $\mathbf{f}$ from the L^2 approximants $\mathbf{p}_n^*$ of degrees $n \le 10$.

degree n	$\|\mathbf{f}-\mathbf{p}_n^*\|$	degree n	$\|\mathbf{f}-\mathbf{p}_n^*\|$
1	1.64791	6	$1.33057 \cdot 10^{-3}$
2	$5.80573 \cdot 10^{-1}$	7	$1.98631 \cdot 10^{-4}$
3	$1.66149 \cdot 10^{-1}$	8	$2.63225 \cdot 10^{-5}$
4	$3.92294 \cdot 10^{-2}$	9	$3.13480 \cdot 10^{-6}$
5	$7.79517 \cdot 10^{-3}$	10	$3.38923 \cdot 10^{-7}$

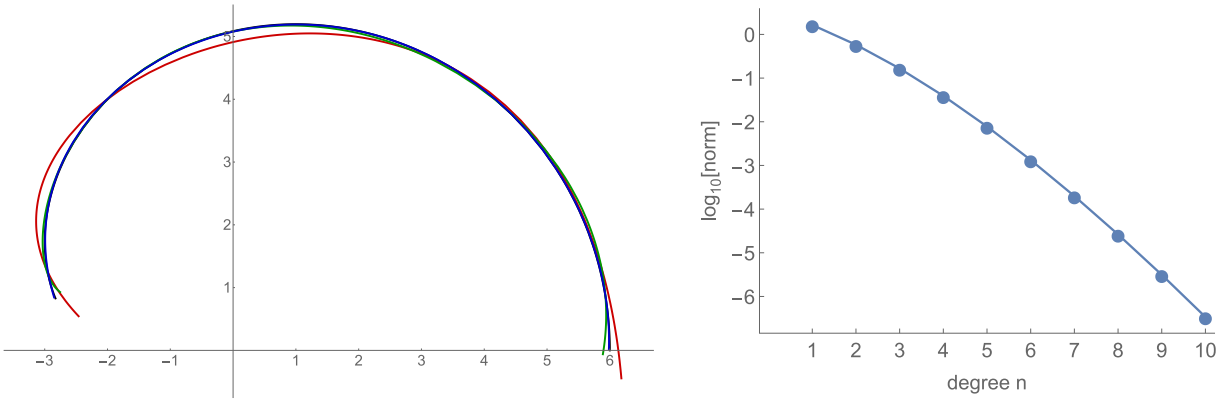

Fig. 1. Left: The curve $\mathbf{f}$ (black) from Example 1 and its L^2 approximants of degree 3 (red), 4 (green) and 5 (blue). Due to small approximation errors, it is difficult to distinguish some approximants from the original curve on the scale of the plot. Right: Graph of the norm $\|\mathbf{f}-\mathbf{p}_n^*\|$ in the logarithmic scale for increasing degrees n. (For interpretation of the references to color in this figure legend, the reader is referred to the web version of this article.)

Example 1. Let $\mathbf{f}$ be a segment of the cardioid curve parameterized as

$$\mathbf{f}(t) = 2\left(2\cos\left(\frac{3\pi t}{4}\right) + \cos\left(\frac{3\pi t}{2}\right)\right) + 2\,\mathrm{i}\left(2\sin\left(\frac{3\pi t}{4}\right) + \sin\left(\frac{3\pi t}{2}\right)\right), \quad t \in [0,1]. \tag{4}$$

Using the Legendre basis (3), we obtain the coefficients $\mathbf{a}_k = \langle \mathbf{f}, L_k \rangle$ of the L^2 approximants $\mathbf{p}_n^*(t)$ for degrees $n \le 10$ as

$$\mathbf{a}_0 = 7.76009 \cdot 10^{-1} + 3.32249\,\mathrm{i}, \quad \mathbf{a}_1 = -3.22868 - 1.43450 \cdot 10^{-1}\,\mathrm{i}, \quad \mathbf{a}_2 = 4.85644 \cdot 10^{-1} - 1.46380\,\mathrm{i},$$
$$\mathbf{a}_3 = 4.80152 \cdot 10^{-1} + 2.80916 \cdot 10^{-1}\,\mathrm{i}, \quad \mathbf{a}_4 = -9.81756 \cdot 10^{-2} + 1.28172 \cdot 10^{-1}\,\mathrm{i},$$
$$\mathbf{a}_5 = -2.89204 \cdot 10^{-2} - 2.53336 \cdot 10^{-2}\,\mathrm{i}, \quad \mathbf{a}_6 = 5.25026 \cdot 10^{-3} - 5.60616 \cdot 10^{-3}\,\mathrm{i},$$
$$\mathbf{a}_7 = 9.45288 \cdot 10^{-4} + 9.15097 \cdot 10^{-4}\,\mathrm{i}, \quad \mathbf{a}_8 = -1.38092 \cdot 10^{-4} + 1.40329 \cdot 10^{-4}\,\mathrm{i},$$
$$\mathbf{a}_9 = -1.85538 \cdot 10^{-5} - 1.84066 \cdot 10^{-5}\,\mathrm{i}, \quad \mathbf{a}_{10} = 2.19929 \cdot 10^{-6} - 2.20799 \cdot 10^{-6}\,\mathrm{i}.$$

This gives $\mathbf{p}_n^*(t) = \sum_{j=0}^{n} \mathbf{a}_k L_k(t)$, $n = 1, 2, \ldots, 10$. The corresponding norms $\|\mathbf{f}-\mathbf{p}_n^*\|$ for $n = 1, 2, \ldots, 10$ are shown in Table 1.

Fig. 1 (left) shows the curve $\mathbf{f}$ (black) and its L^2 approximants of degree 3 (red), 4 (green) and 5 (blue). The error decreases exponentially with the degree, as shown in Fig. 1 (right). Moreover, in Fig. 2 one can see plots of functions $\mathrm{Re}(\mathbf{f}(t)-\mathbf{p}_n^*(t))^2 + \mathrm{Im}(\mathbf{f}(t)-\mathbf{p}_n^*(t))^2$ for $t \in [0,1]$ and $n = 3, 4, 5$.

The polynomial L^2 approximation of curves offers a convenient approximation of a given planar parametric curve. In what follows, we examine how to find these kinds of approximants within the set of planar Pythagorean-hodograph curves. Since we lose the linear space structure, the problem becomes nonlinear and is much more challenging.

3. L^2 approximation using planar Pythagorean-hodograph curves

A planar polynomial Pythagorean-hodograph (PH) curve $\mathbf{p} : [0,1] \to \mathbb{C}$, $\mathbf{p}(t) = x(t) + \mathrm{i}\,y(t)$, is characterized by the property that $|\mathbf{p}'(t)| = \sigma(t)$ for some polynomial $\sigma \in \mathbb{R}[t]$. It is well-known [4] that $\mathbf{p}$ is a PH curve iff its hodograph $\mathbf{h} = \mathbf{p}'$ is given by $\mathbf{h}(t) = \mathbf{w}^2(t)$, $t \in [0,1]$, for some complex-valued polynomial $\mathbf{w}$, called the *preimage*. Thus, to construct a planar PH curve, one chooses a preimage polynomial $\mathbf{w} \in \mathbb{P}_m(\mathbb{C})$,

$$\mathbf{w}(t) = \sum_{j=0}^{m} \mathbf{w}_j b_j^m(t), \quad \mathbf{w}_j = w_{j,1} + \mathrm{i}\,w_{j,2} \in \mathbb{C}, \tag{5}$$

of a given degree m and computes the hodograph

$$\mathbf{h}(t) = \mathbf{w}^2(t) = \sum_{j=0}^{2m} \mathbf{h}_j b_j^{2m}(t), \quad \mathbf{h}_j = h_{j,1} + \mathrm{i}\,h_{j,2} \in \mathbb{C}, \tag{6}$$

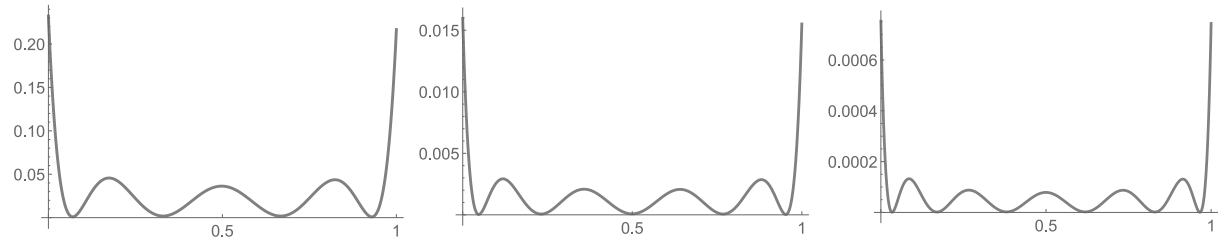

Fig. 2. Plots of functions $\mathrm{Re}(\mathbf{f}(t)-\mathbf{p}_n^*(t))^2+\mathrm{Im}(\mathbf{f}(t)-\mathbf{p}_n^*(t))^2$ for $t\in[0,1]$ and $n=3,4,5$ from Example 1.

where

$$\mathbf{h}_j \;=\; \sum_{k=\max(0,j-m)}^{\min(m,j)} \frac{\binom{m}{k}\binom{m}{j-k}}{\binom{2m}{j}}\,\mathbf{w}_k\mathbf{w}_{j-k}\,,\quad 0\le j\le 2m\,.$$

By integration, we obtain a PH curve of degree $n=2m+1$, i.e.,

$$\mathbf{p}(t)=\sum_{j=0}^{2m+1}\mathbf{p}_j\,b_j^{2m+1}(t),\quad \mathbf{p}_j=p_{j,1}+\mathrm{i}\,p_{j,2}\in\mathbb{C}, \tag{7}$$

where

$$\mathbf{p}_{j+1}=\mathbf{p}_j+\frac{1}{2m+1}\mathbf{h}_j,\quad j=0,1,\ldots,2m,$$

and $\mathbf{p}_0\in\mathbb{C}$ is a free integration constant. Thus, any planar PH curve of odd degree $n=2m+1$ can be constructed with $2m+4$ degrees of freedom. Let

$$\mathcal{PH}_n=\left\{\mathbf{p}:[0,1]\to\mathbb{C};\ \mathbf{p}'=\mathbf{w}^2 \text{ for some } \mathbf{w}\in\mathbb{P}_m(\mathbb{C}),\ m=(n-1)/2\right\}$$

be the set of planar PH curves of odd degree n. Finding the L^2 approximant $\mathbf{p}_n^{*\mathrm{PH}}\in\mathcal{PH}_n$, denoted as the L2–PH approximant, for a given $\mathbf{f}=f_1+\mathrm{i}\,f_2\in C([0,1],\mathbb{C})$ incurs a nonlinear optimization problem. Specifically, from (2) we have

$$\min_{\mathbf{p}\in\mathcal{PH}_n}\|\mathbf{f}-\mathbf{p}\|^2=\min_{\mathbf{p}\in\mathcal{PH}_n}\left\{\int_0^1(f_1(t)-x(t))^2+(f_2(t)-y(t))^2\,dt;\ \mathbf{p}(t)=x(t)+\mathrm{i}\,y(t)\right\}. \tag{8}$$

By (7) the curve $\mathbf{p}$ is uniquely determined by $\mathbf{w}_j$, $j=0,1,\ldots,m$, and $\mathbf{p}_0$. Moreover, the coefficients $\mathbf{p}_j$ depend nonlinearly on the coefficients of the preimage. Solving the minimization problem (8) is thus equivalent to finding the minimum of the nonlinear function Ψ of $2m+4$ real variables defined by

$$\Psi(\mathbf{w}_0,\ldots,\mathbf{w}_m,\mathbf{p}_0)=\Psi(w_{0,1},w_{0,2},\ldots,w_{m,1},w_{m,2},p_{0,1},p_{0,2}):=\int_0^1(f_1(t)-x(t))^2+(f_2(t)-y(t))^2\,dt.$$

This may be further simplified to

$$\Psi(\mathbf{w}_0,\ldots,\mathbf{w}_m,\mathbf{p}_0)=\sum_{j,k=0}^{n}\left(p_{j,1}p_{k,1}+p_{j,2}p_{k,2}\right)\beta_{j,k}-2\sum_{j=0}^{n}\left(p_{j,1}\gamma_{j,1}+p_{j,2}\gamma_{j,2}\right)+\gamma, \tag{9}$$

where we define

$$\beta_{j,k}=\int_0^1 b_j^n(t)b_k^n(t)\,dt,\quad \gamma_{j,1}=\int_0^1 f_1(t)b_j^n(t)\,dt,\quad \gamma_{j,2}=\int_0^1 f_2(t)b_j^n(t)\,dt,\quad \gamma=\int_0^1 f_1^2(t)+f_2^2(t)\,dt. \tag{10}$$

Note that $\beta_{j,k}$ are the elements of the Gram matrix corresponding to the Bernstein basis of $\mathbb{P}_n$, and they satisfy

$$\sum_{k=0}^{n}\beta_{j,k}=\frac{1}{n+1}.$$

The problem can be solved by some nonlinear optimization solver or a Newton–Raphson iteration applied to the nonlinear system of equations

$$\frac{\partial\Psi}{\partial w_{j,\ell}}=0,\quad j=0,1,\ldots,m,\quad \frac{\partial\Psi}{\partial p_{0,\ell}}=0,\quad \ell=1,2, \tag{11}$$

which reduces to

$$\sum_{j,k=0}^{n}\left(p_{j,1}\frac{\partial p_{k,1}}{\partial w_{s,\ell}}+p_{j,2}\frac{\partial p_{k,2}}{\partial w_{s,\ell}}\right)\beta_{j,k}-\sum_{j=0}^{n}\left(\frac{\partial p_{j,1}}{\partial w_{s,\ell}}\gamma_{j,1}+\frac{\partial p_{j,2}}{\partial w_{s,\ell}}\gamma_{j,2}\right)=0,\quad s=0,1,\ldots,m,\quad \ell=1,2,$$

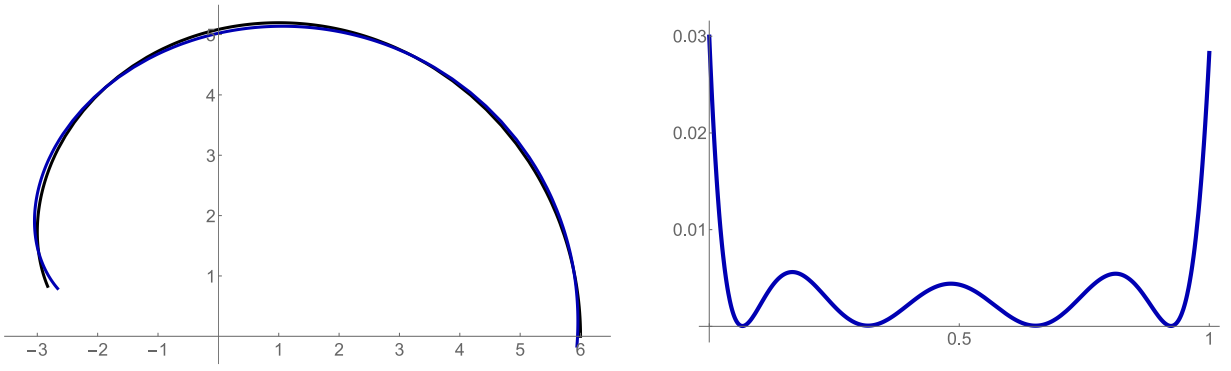

Fig. 3. Left: The given curve $\mathbf{f}$ (black) and its quintic L2–PH approximant $\mathbf{p}_5^{*\text{PH}}$ (blue) from Example 2. Right: The graph of the function $\text{Re}\,(\mathbf{f}(t)-\mathbf{p}_5^{*\text{PH}}(t))^2 + \text{Im}\,(\mathbf{f}(t)-\mathbf{p}_5^{*\text{PH}}(t))^2$ for $t\in[0,1]$. (For interpretation of the references to color in this figure legend, the reader is referred to the web version of this article.)

$$\sum_{j=0}^{n}\left(p_{j,\ell}\sum_{k=0}^{n}\beta_{j,k}-\gamma_{j,\ell}\right)=0,\quad \ell=1,2.$$

Example 2. We demonstrate the construction in the case of a segment of the cardioid curve $\mathbf{f}$ from Example 1. Consider the degree $n=5$. The Bézier coefficients of a quintic PH curve (7) are expressed in terms of Bézier coefficients of the quadratic preimage (5) by

$$\begin{aligned}
&\mathbf{p}_1=\mathbf{p}_0+\frac{1}{5}\,\mathbf{w}_0^2,\quad \mathbf{p}_2=\mathbf{p}_1+\frac{1}{5}\,\mathbf{w}_0\mathbf{w}_1\,,\\
&\mathbf{p}_3=\mathbf{p}_2+\frac{1}{5}\,\frac{2\,\mathbf{w}_1^2+\mathbf{w}_0\mathbf{w}_2}{3}\,,\\
&\mathbf{p}_4=\mathbf{p}_3+\frac{1}{5}\,\mathbf{w}_1\mathbf{w}_2\,,\quad \mathbf{p}_5=\mathbf{p}_4+\frac{1}{5}\,\mathbf{w}_2^2.
\end{aligned}$$

The Gram matrix is

$$(\beta_{j,k})_{j,k=0}^{5}=\frac{1}{2772}\begin{pmatrix}
252 & 126 & 56 & 21 & 6 & 1\\
126 & 140 & 105 & 60 & 25 & 6\\
56 & 105 & 120 & 100 & 60 & 21\\
21 & 60 & 100 & 120 & 105 & 56\\
6 & 25 & 60 & 105 & 140 & 126\\
1 & 6 & 21 & 56 & 126 & 252
\end{pmatrix},$$

and

$$(\gamma_{j,1})_{j=0}^{5}=\begin{pmatrix}
8.33377\cdot 10^{-1}\\
5.54474\cdot 10^{-1}\\
2.28945\cdot 10^{-1}\\
-7.83730\cdot 10^{-2}\\
-3.14647\cdot 10^{-1}\\
-4.47767\cdot 10^{-1}
\end{pmatrix},\quad (\gamma_{j,2})_{j=0}^{5}=\begin{pmatrix}
3.75306\cdot 10^{-1}\\
6.26378\cdot 10^{-1}\\
7.30680\cdot 10^{-1}\\
6.94647\cdot 10^{-1}\\
5.49895\cdot 10^{-1}\\
3.45581\cdot 10^{-1}
\end{pmatrix},\quad \gamma=24.80169.$$

This defines $\Psi(\mathbf{w}_0,\mathbf{w}_1,\mathbf{w}_2,\mathbf{p}_0)$ and by computing its (global) minimum, we obtain the solution

$$\mathbf{w}_0=3.45388+3.19403\,\mathrm{i},\quad \mathbf{w}_1=-1.10742+5.62280\,\mathrm{i},\quad \mathbf{w}_2=-2.71167+1.25205\,\mathrm{i}$$

and

$$\mathbf{p}_0=5.94042-1.62505\cdot 10^{-1}\,\mathrm{i}.$$

The distance between $\mathbf{f}$ and its L2–PH approximant $\mathbf{p}_5^{*\text{PH}}$ equals $\left\|\mathbf{f}-\mathbf{p}_5^{*\text{PH}}\right\|=5.83070\cdot 10^{-2}$. Both curves are shown in Fig. 3 (left). The graph of the function $\text{Re}\,(\mathbf{f}(t)-\mathbf{p}_5^{*\text{PH}}(t))^2+\text{Im}\,(\mathbf{f}(t)-\mathbf{p}_5^{*\text{PH}}(t))^2$ for $t\in[0,1]$ is also shown (right).

Note that due to the nonlinearity of $\Psi(\mathbf{w}_0,\ldots,\mathbf{w}_m,\mathbf{p}_0)$ there might be many local minima, so it is important to choose an appropriate optimization algorithm that finds the global minimum, or to provide good starting values for iterative methods. One way to obtain such values is to use the coefficients of the alternative L^2 approximant, derived in the next section, which is computed through the solution of a linear system of equations.

4. Alternative L^2 approximation using planar Pythagorean-hodograph curves

We now propose an alternative way to construct the PH curve that approximates a given $\mathbf{f} : [0,1] \to \mathbb{C}$ and is close to the nonlinear L2–PH approximant $\mathbf{p}_n^{*\mathrm{PH}} \in \mathcal{PH}_n$, described in the previous section. The basic idea is to make the problem linear by performing the standard linear L^2 approximation in the preimage space rather than directly in $\mathcal{PH}_n$. The idea follows from results presented in [27] that a good approximation in the preimage space yields a good approximation also in $\mathcal{PH}_n$.

However, the first question is how to transform the given curve into the preimage space since the latter is defined only for PH curves. If $\mathbf{f}$ is a polynomial PH curve, a preimage $\mathbf{w}$ exists such that $\mathbf{f}' = \mathbf{w}^2$, which we can write as $\mathbf{w} = \pm\sqrt{\mathbf{f}'}$. Note that $\pm$ solutions are just rotations of each other by $\pm\pi$ in the complex plane. We can apply the same idea to a general parametric curve $\mathbf{f} \in C^1([0,1],\mathbb{C})$ and define the preimage as the complex square root of its derivative $\mathbf{f}'$. However, $\mathbf{w}$ is, in general, no longer polynomial and certain technical details arise in computing the complex square root of a complex function properly to obtain a continuous preimage curve. Specifically, the square root of $\mathbf{z}(t) = z_1(t) + \mathrm{i}\, z_2(t)$ is

$$\pm\sqrt{|\mathbf{z}(t)|}\,\exp\left(\frac{1}{2}\arg\mathbf{z}(t)\,\mathrm{i}\right),$$

where $\arg\mathbf{z}(t) \in (-\pi,\pi]$ is a discontinuous function at points where $\mathbf{z}(t)$ crosses the negative real line. Thus, to retain continuity, we have to switch between the two branches of solutions at these points, as described in Algorithm 1.

Algorithm 1. ComplexSquareRoot

Input: $\mathbf{z}(t) = z_1(t) + \mathrm{i}\, z_2(t)$, $\mathbf{z} \in C([0,1],\mathbb{C})$

1: compute the set Z of all odd multiplicity zeros of z_2 in $(0,1)$
2: compute the subsets Z_1 and Z_2, such that $Z = Z_1 \cup Z_2$, $Z_1 \cap Z_2 = \emptyset$, and $z_1(t_\ell) < 0$ for every $t_\ell \in Z_1$
3: sort the values in Z_1 as $0 < t_1 < t_2 < \cdots < t_L < t_{L+1} := 1$
4: sort the values in Z_2 as $0 < u_1 < u_2 < \cdots < u_K < u_{K+1} := 1$
5: if odd(L) define $I_1 = [0,t_1) \cup [t_2,t_3) \cup \cdots \cup [t_{L-1},t_L)$ else $I_1 = [0,t_1) \cup [t_2,t_3) \cup \cdots \cup [t_L,1]$
6: if odd(K) define $I_2 = [0,u_1) \cup [u_2,u_3) \cup \cdots \cup [u_{K-1},u_K)$, else $I_2 = [0,u_1) \cup [u_2,u_3) \cup \cdots \cup [u_K,1]$
7: define $\chi_1(t) = \begin{cases} 1, & t \in I_1 \\ -1, & \text{else} \end{cases}$, $\chi_2(t) = \begin{cases} 1, & t \in I_2 \\ -1, & \text{else} \end{cases}$
8; compute $\mu = \mathrm{sign}\left(z_2\left(\frac{\min\{t_1,u_1\}}{2}\right)\right)$
9: define $\mathbf{a}(t) = \frac{\sqrt{2}}{2}\left(\chi_1(t)\sqrt{|\mathbf{z}(t)| + z_1(t)} + \mathrm{i}\,\mu\,\chi_2(t)\sqrt{|\mathbf{z}(t)| - z_1(t)}\right)$

Output: $\mathbf{a}(t)$

Using this algorithm, we define the preimage of $\mathbf{f} \in C^1([0,1],\mathbb{C})$ as

$$\mathbf{w}_\mathbf{f}(t) = \textbf{ComplexSquareRoot}(\mathbf{f}'(t)), \quad t \in [0,1].$$

The steps for constructing the approximating PH curve are given in the following algorithm.

Algorithm 2. Alternative-L2–PH approximant

Input: $\mathbf{f} \in C^1([0,1],\mathbb{C})$, degree m

1: compute $\mathbf{w}_\mathbf{f}(t) = \textbf{ComplexSquareRoot}(\mathbf{f}'(t))$
2: compute $G = \left(\left\langle b_k^m,\, b_j^m\right\rangle\right)_{j,k=0}^m$, $\mathbf{g} = \left(\left\langle \mathbf{w}_\mathbf{f},\, b_j^m\right\rangle\right)_{j=0}^m$
3: solve the Gram system $G(\mathbf{w}_j)_{j=0}^m = \mathbf{g}$
4: define the preimage as in Eq. (5)
5: compute the hodograph Eq. (6)
6: choose $\mathbf{p}_0$
7: determine $\mathbf{p}$ by Eq. (7)

Output: PH curve $\mathbf{p}$

The quantities in steps 1–5 of the Algorithm 2 are uniquely defined, but $\mathbf{p}_0$ can be arbitrarily chosen. Since $\mathbf{p}(0) = \mathbf{p}_0$, the simplest way is to interpolate the initial curve point, i.e., $\mathbf{p}_0 = \mathbf{f}(0)$. However, symmetry is not preserved with this simple choice. An alternative is to compute $\mathbf{p}_0$ in the sense of a L^2 approximation, i.e.,

$$\mathbf{p}_0^* = \operatorname*{argmin}_{\mathbf{p}_0 \in \mathbb{C}} \|\mathbf{f} - \mathbf{p}\|\,,$$

where $\mathbf{p}' = \mathbf{w}^2$ for $\mathbf{w}$ computed in step 4 of Algorithm 2. This is a linear problem, and by some computation, we obtain

$$\mathbf{p}_0^* = \left(\sum_{j,k=0}^{n} \beta_{j,k}\right)^{-1} \left(\sum_{j=0}^{n} \begin{bmatrix}\gamma_{j,1}\\ \gamma_{j,2}\end{bmatrix} - \frac{1}{n}\sum_{j=1}^{n}\sum_{\ell=0}^{j-1} \mathbf{h}_\ell \left(\sum_{k=0}^{n} \beta_{j,k}\right)\right) = \sum_{j=0}^{n} \begin{bmatrix}\gamma_{j,1}\\ \gamma_{j,2}\end{bmatrix} - \frac{1}{n(n+1)}\sum_{j=1}^{n}\sum_{\ell=0}^{j-1} \mathbf{h}_\ell, \tag{12}$$

where the notation from (10) is employed. With this choice, we call the resulting degree $n = 2m+1$ curve the *alternative L^2 PH approximant* or AL2–PH approximant and denote it by $\mathbf{p}_n^{*\mathrm{alt}}$.

Lemma 1. *Suppose that $\mathbf{f}$ is a PH curve of degree $n = 2m+1$ obtained from the preimage $\mathbf{w}_\mathbf{f} \in \mathbb{P}_m(\mathbb{C})$. Then $\mathbf{p}_n^{*\mathrm{alt}} = \mathbf{f}$.*

Proof. From the uniqueness of the solution of the Gram system and the fact that $\mathbf{w}_\mathbf{f}$ lies in the subspace $\mathbb{P}_m(\mathbb{C})$, it follows that the L^2 approximant $\mathbf{w}$, computed by Algorithm 2, equals $\mathbf{w} = \mathbf{w}_\mathbf{f}$. Furthermore

$$\min_{\mathbf{p}_0\in\mathbb{C}} \|\mathbf{f}-\mathbf{p}\| = \min_{\mathbf{p}_0\in\mathbb{C}} \left\| \int_0^t \mathbf{w}_\mathbf{f}^2(t)\,dt + \mathbf{f}(0) - \left(\int_0^t \mathbf{w}^2(t)\,dt + \mathbf{p}_0\right)\right\| = \min_{\mathbf{p}_0\in\mathbb{C}} \|\mathbf{f}(0)-\mathbf{p}_0\|,$$

so clearly $\mathbf{p}_0 = \mathbf{f}(0)$, which concludes the proof. □

Example 3. We compare the nonlinear L2–PH approximants from Section 3 with the AL2–PH approximants obtained from Algorithm 2 for the segment of the cardioid curve $\mathbf{f}$ given by (4) in Example 1. First, we compute the preimage $\mathbf{w}_\mathbf{f}$ using Algorithm 1, which gives

$$I_1 = \left[0, \tfrac{4}{9}\right), \quad I_2 = [0,1], \quad \chi_1(t) = \begin{cases} 1, & 0 \le t < \frac{4}{9} \\ -1, & \frac{4}{9} \le t \le 1, \end{cases} \quad \chi_2(t) = 1, \quad \mu = 1,$$

and

$$\mathbf{w}_\mathbf{f}(t) = \sqrt{\frac{3\pi}{2}}\left(\chi_1(t)\sqrt{2\cos\left(\frac{3\pi t}{8}\right) - \sin\left(\frac{3\pi t}{4}\right) - \sin\left(\frac{3\pi t}{2}\right)} + \mathrm{i}\sqrt{2\cos\left(\frac{3\pi t}{8}\right) + \sin\left(\frac{3\pi t}{4}\right) + \sin\left(\frac{3\pi t}{2}\right)}\right).$$

We fix the degree of the preimage polynomial curve (5) as $m = 2$ to get a PH quintic approximant of the given curve. The Gram system

$$\frac{1}{30}\begin{pmatrix} 6 & 3 & 1 \\ 3 & 4 & 3 \\ 1 & 3 & 6 \end{pmatrix}\begin{pmatrix} \mathbf{w}_0 \\ \mathbf{w}_1 \\ \mathbf{w}_2 \end{pmatrix} = \begin{pmatrix} 4.72344\cdot 10^{-1} + 1.23433\,\mathrm{i} \\ -7.29871\cdot 10^{-2} + 1.19404\,\mathrm{i} \\ -5.09621\cdot 10^{-1} + 9.28364\cdot 10^{-1}\,\mathrm{i} \end{pmatrix},$$

for the coefficients of $\mathbf{w}$ yields

$$\mathbf{w}_0 = 3.37912 + 3.14764\,\mathrm{i}, \quad \mathbf{w}_1 = -1.19724 + 5.61069\,\mathrm{i}, \quad \mathbf{w}_2 = -2.51267 + 1.31187\,\mathrm{i},$$

and from (12) we obtain $\mathbf{p}_0 = 5.97917 + 2.74739\cdot 10^{-2}\,\mathrm{i}$. The resulting quintic AL2–PH approximant $\mathbf{p}_5^{*\mathrm{alt}}$ is shown in Fig. 4 together with the graph of the function $\mathrm{Re}\,(\mathbf{f}(t)-\mathbf{p}_5^{*\mathrm{alt}}(t))^2 + \mathrm{Im}\,(\mathbf{f}(t)-\mathbf{p}_5^{*\mathrm{alt}}(t))^2$ for $t \in [0,1]$. The distance between $\mathbf{f}$ and $\mathbf{p}_5^{*\mathrm{alt}}$ is $\left\|\mathbf{f}-\mathbf{p}_5^{*\mathrm{alt}}\right\| = 1.06979\cdot 10^{-1}$.

The distance between $\mathbf{f}$ and the nonlinear quintic L2–PH approximant from Example 2 is slightly smaller than that between $\mathbf{f}$ and its quintic AL2–PH approximant. However, using the preimage Bézier coefficients and $\mathbf{p}_0$ of the latter approximant as starting values for the Newton–Raphson method when solving (11) provides an efficient procedure to compute the nonlinear L2–PH approximant. Table 2 compares the distances of $\mathbf{f}$ from the proposed approximants as the degree m of the preimage increases, where, as explained, $\mathbf{p}_{2m+1}^{*\mathrm{alt}}$ and $\mathbf{p}_{2m+1}^{*\mathrm{PH}}$ denote the alternative and nonlinear L^2 approximants, respectively. The plot of distances (in log-scale) from Fig. 5 shows that $\mathbf{p}_{2m+1}^{*\mathrm{alt}}$ is comparable with $\mathbf{p}_{2m+1}^{*\mathrm{PH}}$.

Example 4. As a further example, we compare the asymptotic accuracy of the AL2–PH and nonlinear L2–PH to the cardioid curve (4) as the curve length decreases. Specifically, we approximate the sequence of curves $\mathbf{f}_h(t) := \mathbf{f}(th)$ for $h = 1/2^k$, $k = 0, 1, \ldots, 7$, and $t \in [0,1]$, we fix the degree m and compute the AL2–PH and nonlinear L2–PH approximants. To give a comparison with non-PH polynomial L^2 approximants, we also compute the approximants $\mathbf{p}_{2m+1}^*$ as explained in Section 2. The results shown in Table 3 for degree $m = 2$ and in Table 4 for degree $m = 3$ indicate that the approximation order is the same for AL2–PH as well as the nonlinear L2–PH approximant, namely it is $m+2$. The approximation order of polynomial L^2 approximants is higher, i.e., $2m+2$, since there are almost twice as many degrees of freedom available for the construction.

Construction of AL2–PH approximants also provides a simple (linear) way to perform degree reduction on the set of PH curves, as demonstrated in the next example.

Example 5. Suppose that $\mathbf{f}$ is a PH curve of degree 11, derived from the preimage polynomial $\mathbf{w}$ of degree 5 with Bézier coefficients

$$\mathbf{w}_0 = 2+3\,\mathrm{i}, \quad \mathbf{w}_1 = 4+2\,\mathrm{i}, \quad \mathbf{w}_2 = 3+0\,\mathrm{i}, \quad \mathbf{w}_3 = 4-6\,\mathrm{i}, \quad \mathbf{w}_4 = 4+\mathrm{i}, \quad \mathbf{w}_5 = 3+3\,\mathrm{i}.$$

Using Algorithm 2 (steps 2–7 with $\mathbf{p}_0$ computed by (12)) we compute AL2–PH curves of degrees $2m+1$, $m = 1,2,3,4,5$. Clearly, $\mathbf{f} = \mathbf{p}_{11}^{*\mathrm{alt}}$ (see Lemma 1). The distances of $\mathbf{f}$ from $\mathbf{p}_3^{*\mathrm{alt}}$, $\mathbf{p}_5^{*\mathrm{alt}}$, $\mathbf{p}_7^{*\mathrm{alt}}$ and $\mathbf{p}_9^{*\mathrm{alt}}$ are equal to 1.58682, $3.07100\cdot 10^{-1}$, $1.33713\cdot 10^{-1}$, $3.49884\cdot 10^{-2}$, respectively. These curves, together with control polygons, are shown in Fig. 6.

Table 2
The distances of $\mathbf{f}$ from the alternative and nonlinear L^2 PH approximants of different degrees $2m+1$.

degree m	$\left\|\mathbf{f}-\mathbf{p}^{*\text{alt}}_{2m+1}\right\|$	$\left\|\mathbf{f}-\mathbf{p}^{*\text{PH}}_{2m+1}\right\|$
1	$6.11604\cdot 10^{-1}$	$3.72470\cdot 10^{-1}$
2	$1.06979\cdot 10^{-1}$	$5.83070\cdot 10^{-2}$
3	$1.18485\cdot 10^{-2}$	$6.73685\cdot 10^{-3}$
4	$8.74688\cdot 10^{-4}$	$5.32351\cdot 10^{-4}$
5	$1.02990\cdot 10^{-4}$	$6.19591\cdot 10^{-5}$

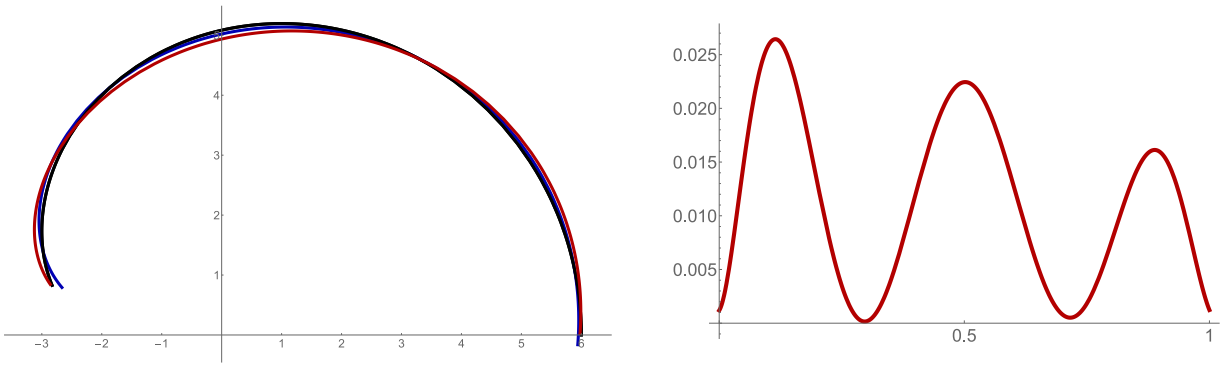

Fig. 4. Left: The given curve $\mathbf{f}$ (black) and its quintic AL2–PH approximant $\mathbf{p}^{*\text{alt}}_5$ (red) in Example 3. The blue curve is the graph of $\mathbf{p}^{*\text{PH}}_5$ from the same example. It is difficult to distinguish the approximants from the original curve on the scale of the plot due to small approximation errors. Right: graph of the function $\text{Re}\,(\mathbf{f}(t)-\mathbf{p}^{*\text{alt}}_5(t))^2+\text{Im}\,(\mathbf{f}(t)-\mathbf{p}^{*\text{alt}}_5(t))^2$ for $t\in[0,1]$. (For interpretation of the references to color in this figure legend, the reader is referred to the web version of this article.)

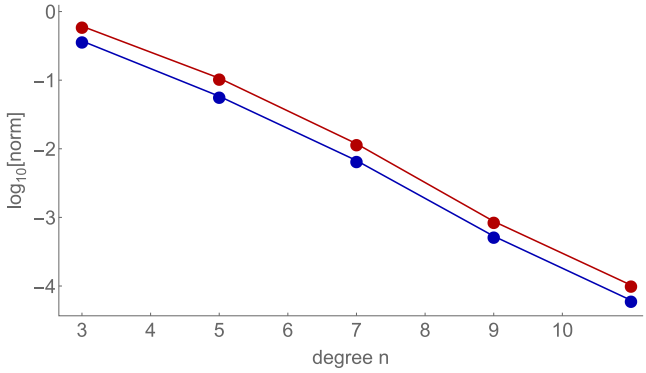

Fig. 5. The plot of distances (in log-scale) given in Table 2 for alternative (red) and nonlinear (blue) L^2 PH approximants. (For interpretation of the references to color in this figure legend, the reader is referred to the web version of this article.)

As shown in Example 4, the distance between the original curve and its L^2 approximants decreases to zero with increasing polynomial degree. However, it is well known that using polynomials of too high degree might lead to some numerical instability. Thus, it is recommended to stay with a low degree and use spline curves instead to increase the number of free parameters.

In the next section, the proposed construction is generalized to Pythagorean-hodograph B-spline curves.

5. L^2 approximation using planar Pythagorean-hodograph B-spline curves

Replacing the subspace of polynomials with the subspace of B-splines to define the preimage curves leads to PH B-spline curves. Planar PH B-spline curves were introduced and examined in [25], and later generalized to the spatial case in [37]. In this section, we use these curves for L^2 approximation.

First, we introduce the notation and review some basics for B-splines.

Table 3
Distances between $\mathbf{f}_h$ and the quintic L^2 PH approximants (AL2–PH and L2–PH) and polynomial L^2 approximants, together with decay exponents (estimated approximation orders).

h	$\left\|\mathbf{f}_h - \mathbf{p}_5^{*\text{alt}}\right\|$	order	$\left\|\mathbf{f}_h - \mathbf{p}_5^{*\text{PH}}\right\|$	order	$\left\|\mathbf{f}_h - \mathbf{p}_5^{*}\right\|$	order
1	$1.06979 \cdot 10^{-1}$	/	$5.83070 \cdot 10^{-2}$	/	$7.79517 \cdot 10^{-3}$	/
$\frac{1}{2}$	$7.06882 \cdot 10^{-3}$	3.91972	$4.12742 \cdot 10^{-3}$	3.82036	$1.40376 \cdot 10^{-4}$	5.79521
$\frac{1}{4}$	$4.47771 \cdot 10^{-4}$	3.98064	$2.65996 \cdot 10^{-4}$	3.95576	$2.27203 \cdot 10^{-6}$	5.94917
$\frac{1}{8}$	$2.80755 \cdot 10^{-5}$	3.99538	$1.67530 \cdot 10^{-5}$	3.98891	$3.58140 \cdot 10^{-8}$	5.98732
$\frac{1}{16}$	$1.75611 \cdot 10^{-6}$	3.99886	$1.04908 \cdot 10^{-6}$	3.99723	$5.60824 \cdot 10^{-10}$	5.99683
$\frac{1}{32}$	$1.09778 \cdot 10^{-7}$	3.99972	$6.55990 \cdot 10^{-8}$	3.99931	$8.76769 \cdot 10^{-12}$	5.99921
$\frac{1}{64}$	$6.86149 \cdot 10^{-9}$	3.99993	$4.10043 \cdot 10^{-9}$	3.99983	$1.37014 \cdot 10^{-13}$	5.99980
$\frac{1}{128}$	$4.28848 \cdot 10^{-10}$	3.99998	$2.56265 \cdot 10^{-10}$	4.00006	$2.14092 \cdot 10^{-15}$	5.99995

Table 4
Distances between $\mathbf{f}_h$ and septic L^2 PH approximants (AL2–PH and L2–PH) and polynomial L^2 approximants, together with decay exponents (estimated approximation orders).

h	$\left\|\mathbf{f}_h - \mathbf{p}_7^{*\text{alt}}\right\|$	order	$\left\|\mathbf{f}_h - \mathbf{p}_7^{*\text{PH}}\right\|$	order	$\left\|\mathbf{f}_h - \mathbf{p}_7^{*}\right\|$	order
1	$1.18485 \cdot 10^{-2}$	/	$6.73685 \cdot 10^{-3}$	/	$1.98631 \cdot 10^{-4}$	/
$\frac{1}{2}$	$4.07488 \cdot 10^{-4}$	4.86180	$2.50142 \cdot 10^{-4}$	4.75125	$8.63644 \cdot 10^{-7}$	7.84544
$\frac{1}{4}$	$1.30158 \cdot 10^{-5}$	4.96842	$8.08766 \cdot 10^{-6}$	4.95088	$3.46480 \cdot 10^{-9}$	7.96152
$\frac{1}{8}$	$4.08960 \cdot 10^{-7}$	4.99216	$2.54808 \cdot 10^{-7}$	4.98824	$1.36248 \cdot 10^{-11}$	7.99039
$\frac{1}{16}$	$1.27974 \cdot 10^{-8}$	4.99804	$7.97881 \cdot 10^{-9}$	4.99709	$5.33107 \cdot 10^{-14}$	7.99760
$\frac{1}{32}$	$4.00053 \cdot 10^{-10}$	4.99951	$2.49425 \cdot 10^{-10}$	4.99949	$2.08332 \cdot 10^{-16}$	7.99940
$\frac{1}{64}$	$1.25027 \cdot 10^{-11}$	4.99988	$3.24424 \cdot 10^{-12}$	6.26458	$8.13880 \cdot 10^{-19}$	7.99985
$\frac{1}{128}$	$3.90718 \cdot 10^{-13}$	4.99997	$9.22569 \cdot 10^{-14}$	5.13608	$3.17930 \cdot 10^{-21}$	7.99996

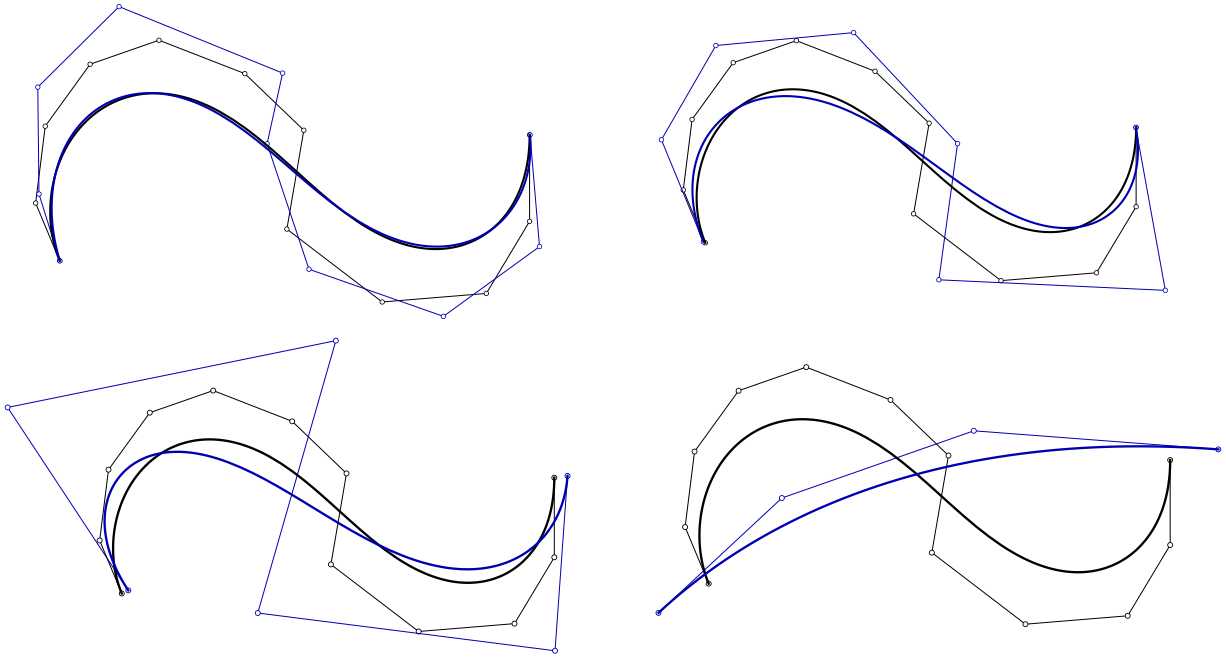

Fig. 6. Degree reduction of the PH curve $\mathbf{f}$ (black) of degree 11 from Example 5 with PH curves (blue) of degrees 9, 7, 5 and 3. (For interpretation of the references to color in this figure legend, the reader is referred to the web version of this article.)

Definition 1. Let $m \in \mathbb{N}_0$ be a chosen degree, $\xi = (\xi_\ell)_{\ell=0}^{N}$, $0 = \xi_0 < \xi_1 < \cdots < \xi_{N-1} < \xi_N = 1$, a given sequence of *breakpoints* and

$$\mathbf{t} = (t_\ell)_{\ell=0}^{d+m+1} = \left(0^{\langle m+1\rangle}, \xi_1^{\langle \nu_1\rangle}, \xi_2^{\langle \nu_2\rangle}, \ldots, \xi_{N-1}^{\langle \nu_{N-1}\rangle}, 1^{\langle m+1\rangle}\right), \quad d = m + \sum_{j=1}^{N-1} \nu_j,$$

the corresponding knot vector, where $\xi_j^{\langle \nu_j\rangle}$ denotes that the breakpoint ξ_j is repeated ν_j-times in the knot sequence. The multiplicity of the knot ν_j satisfies $1 \le \nu_j \le m+1$ for $j = 1, 2, \ldots, N-1$. The jth normalized B-spline basis function of degree m defined over the knot sequence $\mathbf{t}$ is the function $B_{j,\mathbf{t}}^m$ defined recursively as

$$B_{j,\mathbf{t}}^m(t) = \omega_{j,m}(t)\, B_{j,\mathbf{t}}^{m-1}(t) + \left(1 - \omega_{j+1,m}(t)\right) B_{j+1,\mathbf{t}}^{m-1}(t), \qquad \omega_{j,m}(t) := \begin{cases} \frac{t-t_j}{t_{m+j}-t_j}, & t_j \ne t_{m+j}, \\ 0, & \text{otherwise}, \end{cases}$$

with

$$B_{j,\mathbf{t}}^0(t) = \begin{cases} 1, & t \in [t_j, t_{j+1}), \\ 0, & \text{otherwise}, \end{cases} \quad j = 0, 1, \ldots, d-1, \qquad B_{d,\mathbf{t}}^0(t) = \begin{cases} 1, & t \in [t_d, 1], \\ 0, & \text{otherwise}. \end{cases}$$

Furthermore,

$$S_{m,\mathbf{t}} = \operatorname{span}\left\{ B_{0,\mathbf{t}}^m, B_{1,\mathbf{t}}^m, \ldots, B_{d,\mathbf{t}}^m \right\} = \Big\{ f : [0,1] \to \mathbb{R};\ f|_{(\xi_j,\xi_{j+1})} \in \mathbb{P}_m,\ j = 0, 1, \ldots, N-1, \\ \lim_{t \uparrow \xi_j} f^{(\ell)}(t) = \lim_{t \downarrow \xi_j} f^{(\ell)}(t),\ \ell = 0, 1, \ldots, m - \nu_j,\ j = 1, 2, \ldots, N-1 \Big\},$$

is the corresponding spline space with $\dim S_{m,\mathbf{t}} = d+1$.

Remark 1. In Definition 1, the spline space $S_{m,\mathbf{t}}$ is a subspace of real-valued functions in a real variable. However, when dealing with curves, the coefficients are points in $\mathbb{R}^d$, $d \ge 2$, or complex numbers. In order to denote the particular co-domain $\mathbb{F}$, we use the notation $S_{m,\mathbf{t}}(\mathbb{F})$. Note that $S_{m,\mathbf{t}} = S_{m,\mathbf{t}}(\mathbb{R})$, and that $\dim S_{m,\mathbf{t}}(\mathbb{F}) = \dim \mathbb{F}\ \dim S_{m,\mathbf{t}}$. A similar notation has been used for polynomials.

To construct the PH B-spline curve, we choose the preimage $\mathbf{w} \in S_{m,\mathbf{t}}(\mathbb{C})$,

$$\mathbf{w}(t) = \sum_{j=0}^{d} \mathbf{w}_j\, B_{j,\mathbf{t}}^m(t), \quad \mathbf{w}_j = w_{j,1} + \mathrm{i}\, w_{j,2} \in \mathbb{C}, \tag{13}$$

where the knot sequence is chosen as in Definition 1. Further, we compute the hodograph $\mathbf{h} \in S_{2\ m,\widetilde{\mathbf{u}}}(\mathbb{C})$ as

$$\mathbf{h}(t) = \mathbf{w}^2(t) = \sum_{j,\ell=0}^{d} \mathbf{w}_j \mathbf{w}_\ell B_{j,\mathbf{t}}^m(t) B_{\ell,\mathbf{t}}^m(t) = \sum_{j=0}^{d_1} \mathbf{h}_j\, B_{j,\widetilde{\mathbf{u}}}^{2m}(t), \tag{14}$$

with the knot sequence $\widetilde{\mathbf{u}}$ defined as

$$\widetilde{\mathbf{u}} = \left(\widetilde{u}_\ell\right)_{\ell=0}^{d_1+2m+1} = \left(0^{\langle 2m+1\rangle}, \xi_1^{\langle m+\nu_1\rangle}, \xi_2^{\langle m+\nu_2\rangle}, \ldots, \xi_{N-1}^{\langle m+\nu_{N-1}\rangle}, 1^{\langle 2m+1\rangle}\right), \quad d_1 = d + mN.$$

The PH B-spline curve $\mathbf{p}$ is then obtained by the integration

$$\mathbf{p}(t) = \int_0^t \mathbf{h}(\tau)\, d\tau = \sum_{j=0}^{d_2} \mathbf{p}_j\, B_{j,\mathbf{u}}^n(t), \quad n = 2m+1, \quad d_2 = d_1 + 1. \tag{15}$$

This curve is in the spline space $S_{n,\mathbf{u}}(\mathbb{C})$, where $\mathbf{u} = (u_\ell)_{\ell=0}^{d_2+n+1} = (0, \widetilde{\mathbf{u}}, 1)$. Since

$$\mathbf{p}'(t) = \sum_{j=0}^{d_2-1} \frac{n}{\widetilde{u}_{j+n} - \widetilde{u}_j} (\mathbf{p}_{j+1} - \mathbf{p}_j) B_{j,\widetilde{\mathbf{u}}}^{n-1}(t) = \mathbf{h}(t),$$

it follows that the coefficients of $\mathbf{p}$ are equal to

$$\mathbf{p}_{j+1} = \mathbf{p}_j + \delta_{j,n}\, \mathbf{h}_j = \mathbf{p}_0 + \sum_{\ell=0}^{j} \delta_{\ell,n}\, \mathbf{h}_\ell, \quad \delta_{j,n} := \frac{\widetilde{u}_{j+n} - \widetilde{u}_j}{n}, \quad j = 0, 1, \ldots, d_2 - 1,$$

with arbitrary $\mathbf{p}_0$.

Now, following the steps of the Algorithm 2, we compute the Gram matrix and the vector $\mathbf{g}$,

$$G = \left(\left\langle B_{k,\mathbf{t}}^m,\ B_{j,\mathbf{t}}^m \right\rangle \right)_{j,k=0}^{d}, \quad \mathbf{g} = \left(\left\langle \mathbf{w}_\mathbf{f},\ B_{j,\mathbf{t}}^m \right\rangle \right)_{j=0}^{d},$$

where G is now a band matrix. The coefficients of the preimage (13) then follow from the solution of the Gram system $G\left(\mathbf{w}_j\right)_{j=0}^{d} = \mathbf{g}$, and the PH B-spline curve is determined by (14) and (15). As in the case of polynomials, once we fix the preimage, we determine the point $\mathbf{p}_0$ by computing

$$\mathbf{p}_0^* = \operatorname*{argmin}_{\mathbf{p}_0 \in \mathbb{C}} \|\mathbf{f} - \mathbf{p}\|,$$

which yields

$$\mathbf{p}_0^* = \sum_{j=0}^{d_2}\left(\int_0^1 \mathbf{f}(t)B_{j,\mathbf{u}}^n(t)\,dt\right) - \sum_{j=1}^{d_2}\left(\sum_{\ell=0}^{j-1}\delta_{\ell,n}\mathbf{h}_\ell\right)\left(\sum_{k=0}^{d_2}\int_0^1 B_{k,\mathbf{u}}^n(t)B_{j,\mathbf{u}}^n(t)\,dt\right), \tag{16}$$

where we have used the equality

$$\sum_{j,k=0}^{d_2}\int_0^1 B_{j,\mathbf{u}}^n(t)B_{k,\mathbf{u}}^n(t)\,dt = 1.$$

Remark 2. As in the case of L^2 approximation with polynomial PH curves, one can use the computed coefficients of the alternative PH B-spline approximants as starting values for the complicated nonlinear optimization that would give the L^2 PH approximant. The nonlinear function to be minimized is of the same form as (9), where in (10) the Bernstein basis polynomials are replaced with B-splines.

One of the technical issues in the construction of PH B-spline curves is how to express in (14) the coefficients of the hodograph with the coefficients of the preimage. Of course, there are many known algorithms to do this; one of them is described in [25]. However, choosing equidistant breakpoints and the constant multiplicity of inner knots allows us to obtain the explicit formulas. For $\xi_j = j/N$, $j = 0, 1, \ldots, N$, and $\nu_1 = \nu_2 = \cdots = \nu_{N-1} = m - \nu$, the B-splines from Definition 1 are C^ν-continuous, and we denote the corresponding spline space by $S_{m,N}^\nu$. We consider in more detail the following cases: $m = 1$, $\nu = 0$; $m = 2$, $\nu = 1$ and $m = 2$, $\nu = 0$.

The simplest case to be considered is $m = 1$ and $\nu = 0$ with $\dim S_{1,N}^0 = N + 1$, which results in C^1 continuous cubic PH B-spline curves, expressed with B-splines from $S_{3,N}^1$ with $\dim S_{3,N}^1 = 2N + 2$. The coefficients of the hodograph (14) are equal to

$$\mathbf{h}_{2j} = \mathbf{w}_j^2, \quad j = 0, 1, \ldots, N, \quad \mathbf{h}_{2j+1} = \mathbf{w}_j\mathbf{w}_{j+1}, \quad j = 0, 1, \ldots, N-1.$$

Choosing $m = 2$, $\nu = 1$ and $\mathbf{w} \in S_{2,N}^1(\mathbb{C})$, where $\dim S_{2,N}^1 = N + 2$, gives C^2 quintic PH B-spline curves from $S_{5,N}^2(\mathbb{C})$. In this case $\dim S_{5,N}^2 = 3N + 3$, and (14) simplifies to

$$\begin{aligned}
&\mathbf{h}_0 = \mathbf{w}_0^2, \quad \mathbf{h}_1 = \mathbf{w}_0\mathbf{w}_1, \quad \mathbf{h}_2 = \frac{1}{6}\left(\mathbf{w}_0\mathbf{w}_1 + 4\mathbf{w}_1^2 + \mathbf{w}_0\mathbf{w}_2\right),\\
&\mathbf{h}_{3j} = \frac{1}{2}\left(\mathbf{w}_j^2 + \mathbf{w}_j\mathbf{w}_{j+1}\right), \quad \mathbf{h}_{3j+1} = \frac{1}{2}\left(\mathbf{w}_{j+1}^2 + \mathbf{w}_j\mathbf{w}_{j+1}\right), \quad j = 1, 2, \ldots, N-1,\\
&\mathbf{h}_{3j+2} = \frac{1}{12}\left(\mathbf{w}_j\mathbf{w}_{j+1} + 9\mathbf{w}_{j+1}^2 + \mathbf{w}_j\mathbf{w}_{j+2} + \mathbf{w}_{j+1}\mathbf{w}_{j+2}\right), \quad j = 1, 2, \ldots, N-2,\\
&\mathbf{h}_{3N-1} = \frac{1}{6}\left(\mathbf{w}_{N-1}\mathbf{w}_{N+1} + 4\mathbf{w}_N^2 + \mathbf{w}_N\mathbf{w}_{N+1}\right), \quad \mathbf{h}_{3N} = \mathbf{w}_N\mathbf{w}_{N+1}, \quad \mathbf{h}_{3N+1} = \mathbf{w}_{N+1}^2.
\end{aligned}$$

For $m = 2$, $\nu = 0$ the dimension of the preimage spline space equals $\dim S_{2,N}^0 = 2N + 1$ and implies C^1 quintic PH B-spline curves from $S_{5,N}^1(\mathbb{C})$ where $\dim S_{5,N}^1 = 4N + 2$. The coefficients of the hodograph (14) equal

$$\begin{aligned}
&\mathbf{h}_{4j+1} = \mathbf{w}_{2j}\mathbf{w}_{2j+1}, \quad \mathbf{h}_{4j+2} = \frac{1}{3}\left(2\mathbf{w}_{2j+1}^2 + \mathbf{w}_{2j}\mathbf{w}_{2j+2}\right), \quad \mathbf{h}_{4j+3} = \mathbf{w}_{2j+1}\mathbf{w}_{2j+2}, \quad j = 0, 1, \ldots, N-1,\\
&\mathbf{h}_{4j} = \mathbf{w}_{2j}^2, \quad j = 0, 1, \ldots, N.
\end{aligned}$$

The following examples demonstrate the potential of the method.

Example 6. Let us choose $\mathbf{f}$ as the Fermat spiral, parameterized by

$$\mathbf{f}(t) = f_1(t) + \mathrm{i}\, f_2(t) = \sqrt{1+6\pi t}\,\cos(6\pi t) + \mathrm{i}\,\sqrt{1+6\pi t}\,\sin(6\pi t), \quad t \in [0, 1]. \tag{17}$$

Using Algorithm 1, we compute the preimage

$$\mathbf{w}_\mathbf{f}(t) = \frac{\sqrt{2}}{2}\left(\chi_1(t)\sqrt{|\mathbf{f}'(t)| + f_2'(t)} + \mathrm{i}\,\chi_2(t)\sqrt{|\mathbf{f}'(t)| - f_2'(t)}\right), \tag{18}$$

where the sets of intervals that determine $\chi_1(t)$ and $\chi_2(t)$, as described in the algorithm, are

$$I_1 = \{[0, 0.0928728), [0.419641, 0.751748)\}, \quad I_2 = \{[0, 0.254563), [0.585536, 0.918115)\}.$$

Let $S_{1,N}^0(\mathbb{C})$, $S_{2,N}^1(\mathbb{C})$ and $S_{2,N}^0(\mathbb{C})$ be selected for the spline spaces of the preimage curves. As described, this implies PH B-spline curves with parameterizations from $S_{3,N}^1(\mathbb{C})$, $S_{5,N}^2(\mathbb{C})$ and $S_{5,N}^1(\mathbb{C})$, respectively. Choosing $N = 10$ the AL2–PH B-spline approximants are shown in Fig. 7 together with the control polygon and the original curve $\mathbf{f}$. The point $\mathbf{p}_0$ is computed using (16). The errors are $9.36654 \cdot 10^{-2}$, $1.59190 \cdot 10^{-2}$ and $7.31787 \cdot 10^{-3}$, respectively. As stated in Remark 2 we can use the coefficients of these AL2–PH B-spline approximants as starting values for the (complicated) nonlinear optimization for computing the nonlinear L^2 PH B-spline approximants. We obtained the following errors $8.96888 \cdot 10^{-2}$, $1.56043 \cdot 10^{-2}$ and $6.36845 \cdot 10^{-3}$ respectively, which confirm that the alternative approximants provide results very close to optimal. In addition, to show that the approximation properties are similar to those for the polynomial case, Table 5 provides the errors of AL2–PH B-spline approximants from $S_{3,N}^1(\mathbb{C})$, $S_{5,N}^2(\mathbb{C})$ and $S_{5,N}^1(\mathbb{C})$ together with the order of convergence as the number of segments N increases.

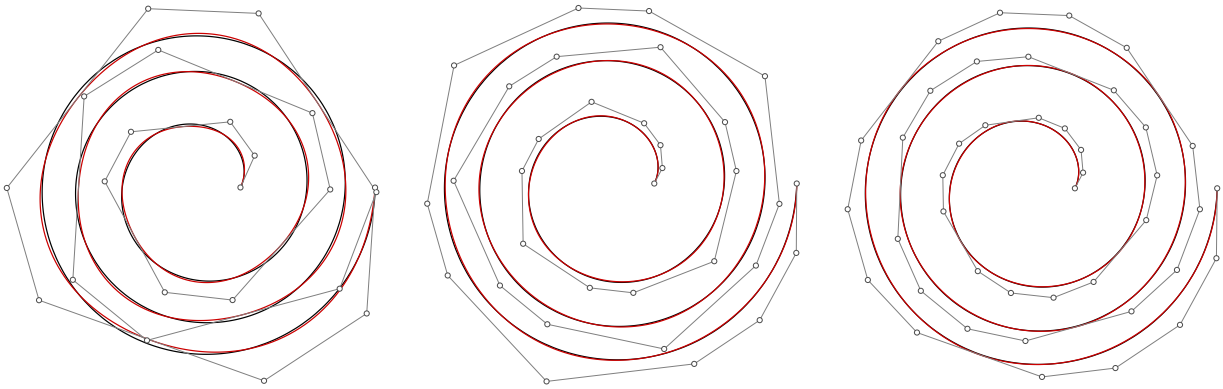

Fig. 7. AL2–PH B-spline approximants (red) from $\mathcal{S}^1_{3,N}(\mathbb{C})$ (left), $\mathcal{S}^2_{5,N}(\mathbb{C})$ (middle) and $\mathcal{S}^1_{5,N}(\mathbb{C})$ (right), together with the control polygon, for the Fermat spiral (17) (black) and $N = 10$ from Example 6. (For interpretation of the references to color in this figure legend, the reader is referred to the web version of this article.)

Table 5
(Example 6) Distances between the Fermat spiral (17) and AL2–PH B-spline approximants from $\mathcal{S}^1_{3,N}(\mathbb{C})$, $\mathcal{S}^2_{5,N}(\mathbb{C})$ and $\mathcal{S}^1_{5,N}(\mathbb{C})$ for different number of segments N together with decay exponents (estimated approximation orders).

	$\mathcal{S}^1_{3,N}(\mathbb{C})$		$\mathcal{S}^2_{5,N}(\mathbb{C})$		$\mathcal{S}^1_{5,N}(\mathbb{C})$	
N	$\|\mathbf{f}-\mathbf{p}^{*\text{alt}}\|$	order	$\|\mathbf{f}-\mathbf{p}^{*\text{alt}}\|$	order	$\|\mathbf{f}-\mathbf{p}^{*\text{alt}}\|$	order
10	$9.36654 \cdot 10^{-2}$	/	$1.59190 \cdot 10^{-2}$	/	$7.31787 \cdot 10^{-3}$	/
20	$8.91885 \cdot 10^{-3}$	3.39259	$6.97852 \cdot 10^{-4}$	4.51168	$5.50769 \cdot 10^{-4}$	3.73190
30	$2.49595 \cdot 10^{-3}$	3.14083	$1.27697 \cdot 10^{-4}$	4.18864	$1.13883 \cdot 10^{-4}$	3.88724
40	$1.031455 \cdot 10^{-3}$	3.07179	$3.92874 \cdot 10^{-5}$	4.09742	$3.67031 \cdot 10^{-5}$	3.93599
50	$5.23012 \cdot 10^{-4}$	3.04343	$1.58812 \cdot 10^{-5}$	4.05912	$1.51765 \cdot 10^{-5}$	3.95760
60	$3.01069 \cdot 10^{-4}$	3.02908	$7.60413 \cdot 10^{-6}$	4.03928	$7.36014 \cdot 10^{-6}$	3.96919
70	$1.88986 \cdot 10^{-4}$	3.02083	$4.08707 \cdot 10^{-6}$	4.02763	$3.98742 \cdot 10^{-6}$	3.97621
80	$1.26342 \cdot 10^{-4}$	3.01565	$2.38931 \cdot 10^{-6}$	4.02023	$2.34334 \cdot 10^{-6}$	3.98083
90	$8.86067 \cdot 10^{-5}$	3.01219	$1.48896 \cdot 10^{-6}$	4.01525	$1.46569 \cdot 10^{-6}$	3.98405

Example 7. As another example we choose $\mathbf{f}$ as the epitrochoid curve, parameterized by

$$\mathbf{f}(t) = f_1(t) + \mathrm{i}\, f_2(t) = 6\cos(2\pi t) - 2\cos(12\pi t) + \mathrm{i}\,(6\sin(2\pi t) - 2\sin(12\pi t)), \quad t \in [0,1]. \tag{19}$$

Using Algorithm 1 we compute the preimage $\mathbf{w}_\mathbf{f}(t)$ as in (18), where the sets of intervals that determine $\chi_1(t)$ and $\chi_2(t)$ are

$$I_1 = \{[0, 0.134005), [0.288483, 0.445331), [0.614789, 0.795412), [0.971986, 1]\},$$
$$I_2 = \{[0, 0.0280138), [0.204588, 0.385211), [0.554670, 0.711517), [0.865995, 1]\}.$$

Further, we split $[0,1]$ with $N+1 = 16$ equidistant breakpoints. The resulting AL2–PH B-spline approximants from $\mathcal{S}^1_{3,N}(\mathbb{C})$, $\mathcal{S}^2_{5,N}(\mathbb{C})$ and $\mathcal{S}^1_{5,N}(\mathbb{C})$ are shown in Fig. 8, together with their control polygons and the original epitrochoid curve. The point $\mathbf{p}_0$ is computed using (16), and the errors are $1.95499 \cdot 10^{-1}$, $6.47254 \cdot 10^{-2}$ and $1.05907 \cdot 10^{-2}$, respectively. Using the coefficients of these AL2–PH B-spline approximants as starting values for the nonlinear optimization (see Remark 2) we compute the *nonlinear* L^2 PH B-spline approximants, for which the errors are equal to $1.86965 \cdot 10^{-1}$, $4.40594 \cdot 10^{-2}$ and $9.2073 \cdot 10^{-3}$, respectively. This again confirms that the alternative L^2 approximant is very close to the optimal one. Again, Table 6 provides the errors of AL2–PH B-spline approximants from $\mathcal{S}^1_{3,N}(\mathbb{C})$, $\mathcal{S}^2_{5,N}(\mathbb{C})$ and $\mathcal{S}^1_{5,N}(\mathbb{C})$ together with the order of convergence as the number of segments N increases.

Although it appears from the figures that the approximating splines form closed curves, this is not the case. The norm of the difference between the first and the last point of the approximants is very small, namely $2.17289 \cdot 10^{-2}$, $2.76544 \cdot 10^{-3}$, $1.02630 \cdot 10^{-4}$, respectively. To obtain the closed approximating curves, the nonlinear condition would need to be incorporated. Since the nonlinearity of this problem is the same as in the case of boundary points interpolation and demands some nontrivial analysis we defer this problem to future consideration.

The last example demonstrates that the proposed approximation scheme gives a simple way to approximate polynomial spline curves with PH spline curves.

Example 8. Let us take $N+1 = 16$ equidistant breakpoints on $[0,1]$ and choose $\mathbf{f}$ as a C^2 cubic spline with control points $(0.01, 0.03)$, $(0.41, 1.3)$, $(0.72, 2.57)$, $(0.78, 4.18)$, $(0.57, 4.71)$, $(0.44, 3.96)$, $(0.55, 2.29)$, $(0.67, 0)$, $(0.51, 0)$, $(0.56, 0.69)$, $(0.69, 1.92)$, $(0.9, 2.59)$, $(1.25, 2.77)$, $(1.58, 1.95)$, $(1.56, 1.25)$, $(1.4, 0.22)$, $(1.82, 0.07)$, $(1.97, 0.62)$ (see Fig. 9). We approximate it with AL2–PH B-splines from $\mathcal{S}^1_{3,N}(\mathbb{C})$, $\mathcal{S}^2_{5,N}(\mathbb{C})$ and $\mathcal{S}^1_{5,N}(\mathbb{C})$, where the point $\mathbf{p}_0$ is computed using (16). The errors are $2.96638 \cdot 10^{-2}$, $2.19907 \cdot 10^{-2}$ and $3.29416 \cdot 10^{-3}$, respectively. The comparison of errors nicely reflects the number of degrees of freedom. Namely, the preimage space dimensions are equal to

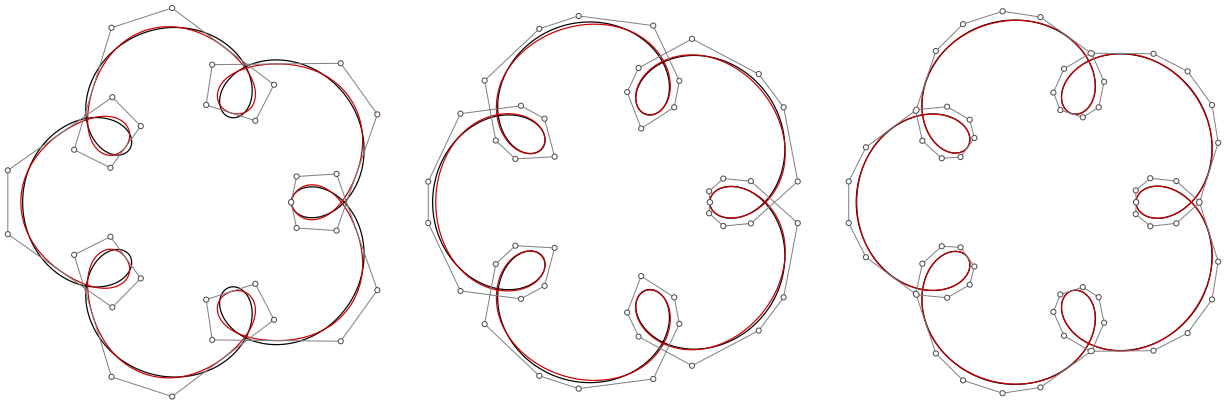

Fig. 8. Example 7: AL2–PH B-spline approximants (red) from $\mathcal{S}^1_{3,N}(\mathbb{C})$ (left), $\mathcal{S}^2_{5,N}(\mathbb{C})$ (middle) and $\mathcal{S}^1_{5,N}(\mathbb{C})$ (right), together with the control polygon, for the epitrochoid curve (19) (black) and $N = 15$. (For interpretation of the references to color in this figure legend, the reader is referred to the web version of this article.)

Table 6
Distances between the epitrochoid curve (19) and AL2–PH B-spline approximants from $\mathcal{S}^1_{3,N}(\mathbb{C})$, $\mathcal{S}^2_{5,N}(\mathbb{C})$ and $\mathcal{S}^1_{5,N}(\mathbb{C})$ for different number of segments N together with decay exponents (estimated approximation orders).

	$\mathcal{S}^1_{3,N}(\mathbb{C})$		$\mathcal{S}^2_{5,N}(\mathbb{C})$		$\mathcal{S}^1_{5,N}(\mathbb{C})$	
N	$\|\mathbf{f} - \mathbf{p}^{*\text{alt}}\|$	order	$\|\mathbf{f} - \mathbf{p}^{*\text{alt}}\|$	order	$\|\mathbf{f} - \mathbf{p}^{*\text{alt}}\|$	order
20	$6.32643 \cdot 10^{-2}$	/	$2.10298 \cdot 10^{-2}$	/	$3.99654 \cdot 10^{-3}$	/
30	$1.53219 \cdot 10^{-2}$	3.49731	$4.23295 \cdot 10^{-3}$	3.95358	$9.91488 \cdot 10^{-4}$	3.43797
40	$5.91753 \cdot 10^{-3}$	3.30700	$1.18965 \cdot 10^{-3}$	4.41194	$3.49429 \cdot 10^{-4}$	3.62520
50	$2.89442 \cdot 10^{-3}$	3.20483	$4.06677 \cdot 10^{-4}$	4.81034	$1.50957 \cdot 10^{-4}$	3.76130
60	$1.63256 \cdot 10^{-3}$	3.14080	$1.62336 \cdot 10^{-4}$	5.03697	$7.50649 \cdot 10^{-5}$	3.83191
70	$1.01232 \cdot 10^{-3}$	3.10023	$7.42408 \cdot 10^{-5}$	5.07527	$4.13586 \cdot 10^{-5}$	3.86681
80	$6.71499 \cdot 10^{-4}$	3.07408	$3.82462 \cdot 10^{-5}$	4.96715	$2.46162 \cdot 10^{-5}$	3.88581
90	$4.68476 \cdot 10^{-4}$	3.05671	$2.17609 \cdot 10^{-5}$	4.78786	$1.55532 \cdot 10^{-5}$	3.89814

$\dim \mathcal{S}^0_{1,N} = 16$, $\dim \mathcal{S}^1_{2,N} = 17$ and $\dim \mathcal{S}^0_{2,N} = 31$. The nonlinear L^2 PH B-spline interpolants have the errors equal to $2.34259 \cdot 10^{-2}$, $1.79251 \cdot 10^{-2}$ and $2.77018 \cdot 10^{-3}$.

6. Conclusion

A general approach to the problem of L^2 approximation of planar curves has been proposed, and the case of approximation by PH curves was studied in detail. Since L^2 approximation by PH curves is a nonlinear optimization problem, an alternative approach was developed, based on minimizing the distance between the preimage polynomial of a PH curve and the complex square root of the derivative of the given curve. The best alternative approximant using this approach is the solution of a *linear* system of equations. An extension of the approach to approximation with PH B-spline curves was also addressed. Several numerical examples demonstrate the potential of the proposed method.

A possible topic for further research would be to impose some additional point interpolation constraints, and to consider the influence of the parameterization of the given curve on the approximation accuracy. Another possible extension would be to consider L^2 approximation for discrete sets of data points, rather than continuous curves. Finally, a generalization of the approach to L^2 approximation of space curves by spatial polynomial PH curves and spatial PH B-spline curves are also of interest.

CRediT authorship contribution statement

Rida T. Farouki: Writing – review & editing, Writing – original draft, Methodology, Investigation, Formal analysis, Conceptualization. **Marjeta Knez:** Writing – review & editing, Writing – original draft, Software, Methodology, Investigation, Formal analysis, Conceptualization. **Vito Vitrih:** Writing – review & editing, Writing – original draft, Methodology, Investigation, Formal analysis, Conceptualization. **Emil Žagar:** Writing – review & editing, Writing – original draft, Methodology, Investigation, Formal analysis, Conceptualization.

Acknowledgments

The second and the fourth authors have been partly supported by the research program P1-0288 and the research grants N1–0137,N1–0237 and J1–3005 by the Slovenian Research and Innovation Agency. The third author has been partly supported by the research program P1–0404 and the research grants N1–0296 and J1–4414 by the Slovenian Research and Innovation Agency.

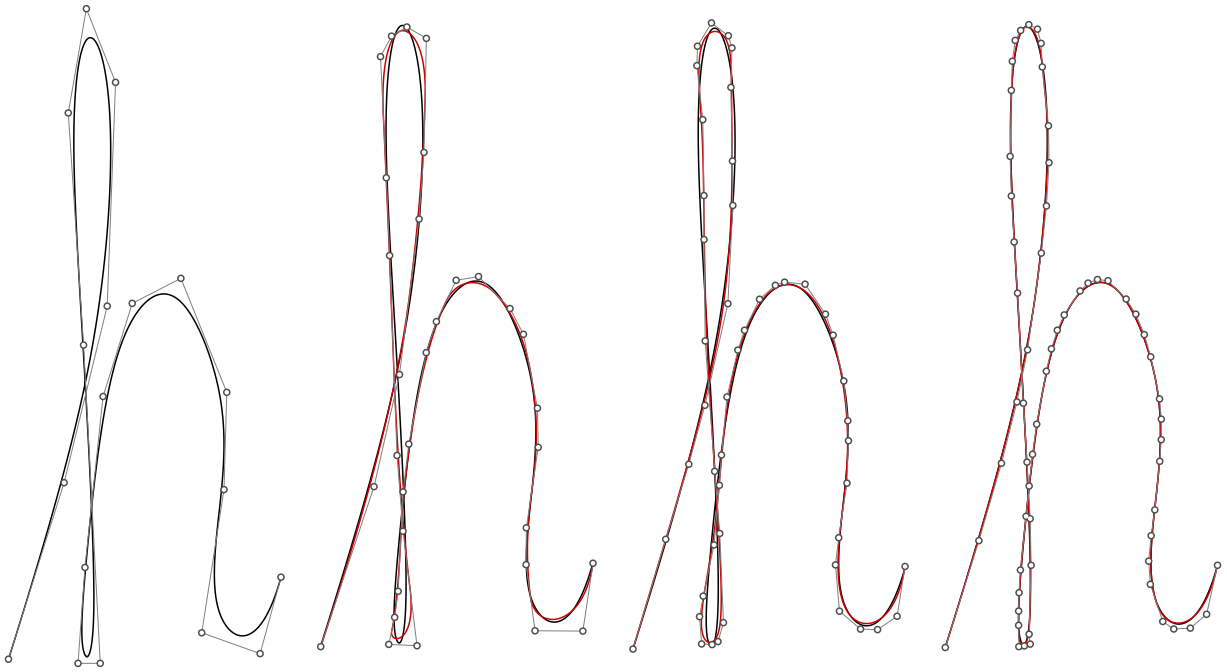

Fig. 9. Example 8: AL2–PH B-spline approximants (red) from $\mathcal{S}^1_{3,N}(\mathbb{C})$ (second plot), $\mathcal{S}^2_{5,N}(\mathbb{C})$ (third plot) and $\mathcal{S}^1_{5,N}(\mathbb{C})$ (fourth plot), together with the control polygon, for the C^2 cubic spline curve (19) (black) and $N = 15$. (For interpretation of the references to color in this figure legend, the reader is referred to the web version of this article.)

References

[1] R.T. Farouki, T. Sakkalis, Pythagorean hodographs, IBM J. Res. Develop. 34 (1990) 736–752.
[2] R.T. Farouki, Pythagorean–Hodograph Curves: Algebra and Geometry Inseparable, Springer, Berlin, 2008.
[3] R.T. Farouki, C. Giannelli, A. Sestini, New Developments in Theory, Algorithms, and Applications for Pythagorean–Hodograph Curves, Advanced Methods for Geometric Modeling and Numerical Simulation, Springer, ISBN: 978-3-030-27331-6, 2019, pp. 127–177,
[4] R.T. Farouki, The conformal map $z \to z^2$ of the hodograph plane, Comput. Aided Geom. Design 11 (1994) 363–390.
[5] H.I. Choi, D.S. Lee, H.P. Moon, Clifford algebra, spin representation, and rational parameterization of curves and surfaces, Adv. Comp. Math. 17 (2002) 5–48.
[6] R.T. Farouki, M. al Kandari, T. Sakkalis, Structural invariance of spatial Pythagorean hodographs, Comput. Aided Geom. Design 19 (2002) 395–407.
[7] B. Bastl, M. Bizzarri, M. Krajnc, M. Lávicka, K. Slabá, Z. Šír, V. Vítrih, E. Žagar, C^1 Hermite interpolation with spatial Pythagorean–hodograph cubic biarcs, J. Comput. Appl. Math. 257 (2014) 65–78.
[8] R.T. Farouki, C. Giannelli, C. Manni, A. Sestini, Identification of spatial PH quintic Hermite interpolants with near–optimal shape measures, Comput. Aided Geom. Design 25 (2008) 274–297.
[9] R.T. Farouki, C.A. Neff, Hermite interpolation by Pythagorean–hodograph quintics, Math. Comp. 64 (1995) 1589–1609.
[10] G. Jaklič, J. Kozak, M. Krajnc, V. Vítrih, E. Žagar, Geometric Lagrange interpolation by planar cubic Pythagorean hodograph curves, Comput. Aided Geom. Design 25 (2008) 720–728.
[11] B. Jüttler, Hermite interpolation by Pythagorean–hodograph curves of degree seven, Math. Comp. 70 (2001) 1089–1111.
[12] S.H. Kwon, Solvability of G^1 Hermite interpolation by spatial Pythagorean–hodograph cubics and its selection scheme, Comput. Aided Geom. Design 27 (2010) 138–149.
[13] A. Sestini, L. Landolfi, C. Manni, On the approximation order of a space data–dependent PH quintic Hermite interpolation scheme, Comput. Aided Geom. Design 30 (2013) 148–158.
[14] Z. Šír, R. Feichtinger, B. Jüttler, Approximating curves and their offsets using biarcs and Pythagorean–hodograph quintics, Comput. Aided Design 38 (2006) 608–618.
[15] Z. Šír, B. Jüttler, C^2 Hermite interpolation by Pythagorean–hodograph space curves, Math. Comp. 76 (2007) 1373–1391.
[16] M. Aigner, Z. Šír, B. Jüttler, Evolution-based least-squares fitting using Pythagorean hodograph spline curves, Comput. Aided Geom. Design 24 (2007) 310–322.
[17] G. Albrecht, R.T. Farouki, Construction of C^2 Pythagorean–hodograph interpolating splines by the homotopy method, Adv. Comp. Math. 5 (1996) 417–442.
[18] G. Jaklič, J. Kozak, M. Krajnc, V. Vítrih, E. Žagar, On interpolation by planar G^2 Pythagorean–hodograph spline curves, Math. Comp. 79 (2010) 305–326.
[19] F. Pelosi, M.L. Sampoli, R.T. Farouki, C. Manni, A control polygon scheme for design of planar C^2 PH quintic spline curves, Comput. Aided Geom. Design 24 (2007) 28–52.
[20] R.T. Farouki, Construction of G^1 planar Hermite interpolants with prescribed arc lengths, Comput. Aided Geom. Design 46 (2016) 64–75.
[21] R.T. Farouki, Existence of Pythagorean–hodograph quintic interpolants to spatial G^1 Hermite data with prescribed arc lengths, J. Symb. Comput. 95 (2019) 202–216.
[22] R.T. Farouki, F. Pelosi, M.L. Sampoli, Approximation of monotone clothoid segments by degree 7 Pythagorean–hodograph curves, J. Comput. Appl. Math. 382 (2021) 113110.
[23] M. Huard, R.T. Farouki, N. Sprynski, L. Biard, C^2 interpolation of spatial data subject to arc–length constraints using Pythagorean–hodograph quintic splines, Graph. Models 76 (2014) 30–42.

[24] M. Knez, F. Pelosi, M.L. Sampoli, Construction of G^2 planar Hermite interpolants with prescribed arc lengths, Appl. Math. Comput. 426 (2022) 127092.
[25] G. Albrecht, C.V. Beccari, J.-C. Canonne, L. Romani, Planar Pythagorean–hodograph B–spline curves, Comput. Aided Geom. Design 57 (2017) 57–77.
[26] R.T. Farouki, Identifying Pythagorean–hodograph curves closest to prescribed Bézier curves, Comput. Aided Design 149 (2022) 103266.
[27] R.T. Farouki, M. Knez, V. Vítrih, E. Žagar, Application of a metric for complex polynomials to bounded modification of planar Pythagorean–hodograph curves, Comput. Aided Geom. Design (2024) submitted.
[28] H. Pottmann, Rational curves and surfaces with rational offsets, Comput. Aided Geom. Design 12 (1995) 175–192.
[29] H. Pottmann, Curve design with rational Pythagorean hodograph curves, Adv. Comp. Math. 3 (1995) 147–170.
[30] L. Romani, F. Montagner, Algebraic–trigonometric Pythagorean–hodograph space curves, Adv. Comp. Math. 45 (2019) 75–98.
[31] L. Romani, L. Saini, G. Albrecht, Algebraic–trigonometric Pythagorean–hodograph curves and their use for Hermite interpolation, Adv. Comp. Math. 40 (2014) 977–1010.
[32] H.I. Choi, C.Y. Han, H.P. Moon, K.H. Roh, N-S. Wee, Medial axis transform and offset curves by Minkowski Pythagorean hodograph curves, Comput. Aided Design 31 (1999) 59–72.
[33] J. Kosinka, B. Jüttler, G^1 Hermite interpolation by Minkowski Pythagorean–hodograph cubics, Comput. Aided Geom. Design 23 (2006) 401–418.
[34] H.P. Moon, Minkowski Pythagorean hodographs, Comput. Aided Geom. Design 16 (1999) 739–753.
[35] W. Gautschi, Numerical Analysis, Birkhäuser, Boston, 1997.
[36] R.T. Farouki, Legendre–Bernstein basis transformations, J. Comput. Appl. Math. 119 (2000) 145–160.
[37] G. Albrecht, C.V. Beccari, L. Romani, Spatial Pythagorean–hodograph B–spline curves and 3D point data interpolation, Comput. Aided Geom. Design 80 (2020) 101868.